Eur. J. Mineral.
2007, **19**, 229–245

Chopinite, $[(Mg,Fe)_3\square](PO_4)_2$, a new mineral isostructural with sarcopside, from a fluorapatite segregation in granulite-facies paragneiss, Larsemann Hills, Prydz Bay, East Antarctica

EDWARD S. GREW[1,*], THOMAS ARMBRUSTER[2], OLAF MEDENBACH[3], MARTIN G. YATES[1] and CHRISTOPHER J. CARSON[4]

[1]Department of Earth Sciences, University of Maine, 5790 Bryand Research Center, Orono, Maine 04469-5790, USA
*Corresponding author, e-mail: esgrew@maine.edu
[2]Laboratorium für chemische und mineralogische Kristallographie, Universität Bern, Freiestrasse 3, 3012 Bern, Switzerland
[3]Institut für Geowissenschaften/Mineralogie, Ruhr-Universität Bochum, 44780 Bochum, Germany
[4]Research School of Earth Sciences, Australian National University, Canberra, ACT 0200, Australia

Abstract: Chopinite, the Mg-dominant analogue of sarcopside, is a new mineral corresponding to synthetic $Mg_3(PO_4)_2$-II, a high-pressure polymorph of the meteoritic mineral farringtonite. A representative electron-microprobe analysis is SiO_2 0.32, P_2O_5 47.32, Al_2O_3 0.05, MgO 30.35, MnO 0.15, FeO 20.99, CaO 0.35, F 0.02, Cl 0.01, Sum 99.54 wt%, which gives $Ca_{0.02}Mg_{2.20}Fe_{0.86}Mn_{0.01}Si_{0.02}P_{1.95}O_8$. Single-crystal X-ray diffraction gives monoclinic symmetry, $P2_1/c$, a = 5.9305(7) Å, b = 4.7583(6) Å, c = 10.2566(10) Å, β = 90.663(9)°, V 289.41(6) Å^3, calculated density 3.34 g/cm^3, Z = 2. Chopinite is of the olivine structure type, but with ordered vacancies and strongly distorted octahedra due to the valence 5+ for P, which results in marked ordering of Mg at M2, whereas Fe^{2+} concentrates at M1, most likely because of its axial symmetry. The strongest lines in the powder pattern [d in Å, (I_{calc}), (hkl)] are 5.92 (42) (100), 3.84(100) (102), 3.48(52) (11$\bar{1}$, 012, 111), 2.51(72) (11$\bar{3}$, 113), 2.44 (73) (21$\bar{1}$, 211). Chopinite is colorless and transparent, biaxial (–), α 1.595(2), β 1.648(2), γ 1.656(2) (589 nm). $2V_x$ (meas.) = 40(2)°, $2V_x$ (calc.) = 41°; $X // b$, $Z \wedge a \sim 55°$. Chopinite is found as four inclusions isolated in a fluorapatite segregation in a quartz mass in a paragneiss from Brattnevet, Larsemann Hills, East Antarctica. Grains are mostly anhedral and range from 0.1 × 0.3 mm to 0.2 × 0.6 mm in size. Minerals present in the chopinite-bearing specimen include wagnerite-*Ma5bc*, xenotime-(Y), stornesite-(Y), P-bearing K-feldspar and plagioclase, Ti-rich biotite, sillimanite, orthopyroxene, sapphirine, hercynite, and corundum. It is inferred to have formed as a result of high melt P concentrations by reaction of biotite with an anatectic melt in which P/Ca ratio exceeded that buffered by apatite saturation due to the very slow diffusion of P relative to Ca in anatectic melt.

Key-words: phosphate, new mineral, Antarctica, Larsemann Hills, electron microprobe, crystal structure, granulite facies, anatexis.

Introduction

Sarcopside, $(Fe, Mn, Mg)_3(PO_4)_2$, is an uncommon mineral in granite pegmatites and in IIIAB meteorites; there are also possible occurrences in metamorphic environments and pallasites. Sarcopside is invariably dominated by Fe, with the maximum X_{Mg} = Mg/(Mg+Fe) = 0.37 and maximum X_{Mn} = Mn/(Mn+Fe) = 0.36. With rare exceptions terrestrial sarcopside forms intergrowths with graftonite or triphylite. The Mg-analogue of sarcopside was first synthesized as a metastable phase by a solid-state exchange process at 660°C and 1 bar by Berthet *et al.* (1972), and subsequently at 600 °C and 30 kbar, by Annersten & Nord (1980). Brunet & Vielzeuf (1996) and Brunet *et al.* (1998) showed that the Mg-analogue of sarcopside is a high-pressure polymorph of the meteoritic mineral farringtonite and determined the equilibrium reaction to lie at 6.32–8.30 kbar for 566–824 °C.

Here we report Mg-dominant analogue of sarcopside as the new mineral chopinite from a terrestrial metamorphic environment: a fluorapatite segregation in granulite-facies (800–860 °C, 6–7 kbar) biotite-quartz-plagioclase paragneiss at 69° 24.437' S, 76° 15.057' E on Brattnevet Peninsula, Larsemann Hills, Prydz Bay, East Antarctica. The mineral and name were approved by the Commission on New Minerals and Mineral Names, International Mineralogical Association (2006-004). The name is for Christian Chopin (born 1955) of the Ecole Normale Supérieure, Paris, France, for his major contributions to the mineralogy of phosphates. Holotype material (sample no. 121401E and thin section 121401E4) is deposited in the Musée de Minéralogie, Ecole des Mines de Paris as catalogue number M 73096.

0935-1221/07/0019-1712 $ 7.65
DOI: 10.1127/0935-1221/2007/0019-1712

Analytical methods

The optical properties of chopinite grain #3 were measured at the Ruhr-Universität Bochum by routine immersion procedure using a microrefractometer spindle-stage (Medenbach, 1985).

X-ray powder-diffraction data were obtained from chopinite grain #3 with a 57.3 mm diameter Gandolfi camera and Cu$K\alpha$ radiation at the Ruhr-Universität Bochum (Table 1).

Cell dimensions of chopinite grain #3 (Table 2) were refined from reflections at scattering angles $13 < \theta < 20°$ obtained with graphite-monochromated Mo$K\alpha$ radiation on an ENRAF NONIUS CAD4 diffractometer equipped with a point detector at the Universität Bern. CAD4 instrumentation gives higher accuracy albeit similar precision as the CCD instrument.

Single-crystal X-ray intensity data were collected on chopinite grain #3 with a 3-circle SMART BRUKER CCD 1K, graphite-monochromated Mo$K\alpha$ radiation at the Universität Bern. Like sarcopside, chopinite is pseudo-orthorhombic, but truly monoclinic. We chose the standard setting $P2_1/c$. Twinning (imitating orthorhombic symmetry) is evident from optical inspection and structure refinement leaving the choice between (100) and (001) as twin planes. Due to $\beta = 90.66°$ (close to 90°) the twin law was not obvious from the single-crystal diffraction pattern. The half-widths of *hk*0 and 0*kl* reflections were checked and the *hk*0 reflections were systematically found to be more asymmetric and broadened compared to 0*kl* reflections, which suggests that the twin plane is {100}, *i.e.*, identical to the twin plane {001} reported by Hurlbut (1965) for sarcopside in the $P2_1/a$ setting. In order to deal with the extensive polysynthetic twinning, a large window for intensity integration for each reflection was chosen. It was then possible to collect the intensity of all twin domains. The structure was solved by direct methods and refined using the SHELXTL Version 6.12 program package (Sheldrick, 1997). All sites were refined with neutral atom scattering-factors (Mg, Fe, P, and O) and anisotropic displacement parameters. In addition, variation of Mg and Fe on the octahedral sites M1 and M2 was allowed assuming complete occupancy. The octahedral site M1' at 0,0,1/2, which is occupied in forsterite

Table 1. X-ray powder-diffraction data for chopinite (grain 3).

I_{est}	d_{meas} (Å)	I_{calc}	d_{calc} (Å)	*hkl*
st	**5.92**	42	5.9306	1 0 0
w	4.31	29	4.3162	0 1 1
st	**3.84**	100	3.8571	1 0 2
vw	3.65			
st	**3.48**	4	3.4979	1 1 $\overline{1}$
		11	3.4879	0 1 2
		37	3.4817	1 1 1
w	2.97	25	2.9653	2 0 0
m	2.77	46	2.7764	0 1 3
st	**2.51**	59	2.5236	1 1 $\overline{3}$
		13	2.5055	1 1 3
st	**2.44**	40	2.4497	2 1 $\overline{1}$
		33	2.4385	2 1 1
m	2.26	11	2.2680	2 1 $\overline{2}$
		17	2.2572	0 1 4
		7	2.2505	2 1 2
w	2.15	7	2.1604	1 2 $\overline{1}$
		13	2.1566	1 2 1
w	1.79	8	1.8006	3 1 $\overline{1}$
		12	1.7898	1 1 5
m	1.74	17	1.7490	2 2 $\overline{2}$
		8	1.7440	0 2 4
		16	1.7409	2 2 2
vw	1.65	15	1.6696	1 2 4
		13	1.6476	1 0 $\overline{6}$
w	1.47	10	1.4884	2 0 $\overline{6}$
		14	1.4827	4 0 0
		8	1.4736	2 0 6
w	1.40	6	1.4003	0 1 7
		7	1.3997	1 3 $\overline{3}$
vw	1.35	5	1.3511	2 3 $\overline{2}$
		5	1.3474	2 3 2

Note: Intensities are visual estimates. Five strongest lines are given in bold. Calculated data from LAZY PULVERIX (Yvon *et al.*, 1977) based on single-crystal refinement: $a = 5.9305(7)$ Å, $b = 4.7583(6)$ Å, $c = 10.2566(10)$ Å, $\beta = 90.663(9)°$

Table 2. Parameters for X-ray data collection and crystal-structure refinement of chopinite.

Diffractometer	Siemens Smart CCD
X-ray radiation	Mo$K\alpha$ (0.71073 Å)
X-ray power	50 kV, 40 mA
Temperature	293 K
Crystal size (mm^3)	0.1 × 0.1 × 0.03
Detector to sample distance	5.4 cm
Rotation axis	ω
Rotation width	0.3°
Total number of frames	1362
Frame size	512 × 512 pixels
Time per frame	120 sec
Space group	$P2_1/c$ (Nr. 14)
Cell dimensions	$a = 5.9305(7)$ (Å)
	$b = 4.7583(6)$ (Å)
	$c = 10.2566(10)$ (Å)
	$\beta = 90.663(9)°$
	$V = 289.41(6)$ Å^3
	$Z = 2$
Collection mode	automated hemisphere
Reflections collected	1543
Maximum 2 θ	55.43
Index range	$-7 \le h \le 5$
	$-6 \le k \le 4$
	$-11 \le l \le 12$
Unique reflections	617
Reflections > 2σ(I)	567
R_{int}	0.028
R_σ	0.027
Number of least squares parameters	64
GooF	1.034
$R1$, I > 2 σ(I)	0.024
$R1$, all data	0.027
w$R2$ (on F^2)	0.058
$+\Delta e$ (e/Å^3)	0.4
$-\Delta e$ (e/Å^3)	0.4

and fayalite, was found to be vacant, or very nearly so. The twin contribution was refined to 17.1(2) %. Anisotropic and isotropic displacement parameters, atomic coordinates and occupancies are given in Tables 3–5.

Chopinite and associated minerals in sections of sample 121401E were analyzed with a Cameca SX-100 electron microprobe at the University of Maine and with a Cameca SX-50 at the Centre de Microanalyse Camparis, Paris. Analytical conditions for analysis of phosphates at the University of Maine were 15 kV accelerating voltage, 10 nA beam current and 20 μm spot diameter, and data were processed using the X-Phi correction of Merlet (1994). The standards used for chopinite and wagnerite were fluorapatite (F*K*α), tugtupite (Na*K*α), synthetic $Mg_3(PO_4)_2$ (Mg*K*α), albite (Al*K*α), albite (Si*K*α), synthetic $Mg_3(PO_4)_2$ (P*K*α), tugtupite (Cl*K*α), fluorapatite (Ca*K*α), rutile (Ti*K*α), rhodonite (Mn*K*α), almandine (Fe*K*α); additionally for apatite, fluorapatite (P*K*α), barite (S*K*α), celestine (Sr*L*α), synthetic Y-Al garnet (Y*L*α), synthetic rare-earth element phosphates (REE *L*α), and U metal (U*M*β). Three grains of chopinite were analyzed at twenty spots where each constituent was counted for 5 seconds, but 4 to 9 analyses were rejected because of impurities and alteration. Fluorine in biotite was analyzed using the TAP crystal and a polylithionite standard. Zr content of rutile was counted for a total of 1600 seconds using a zirconia standard (SPI-47) and 4 spectrometers simultaneously to improve the statistics.

Analytical conditions for analysis of silicates and oxides at the Centre de Microanalyse Camparis were 15 kV accelerating voltage, 10 nA beam current and 5 μm spot diameter, and data were processed using PAP corrections. The standards and counting times used for chopinite, wagnerite and biotite were Durango fluorapatite or topaz (15 s, F*K*α), albite (10 s, Na*K*α), synthetic $Mg_3(PO_4)_2$, (10 s, Mg*K*α), orthoclase (15 s, Al*K*α), diopside (15 s, Si*K*α), synthetic $Mg_3(PO_4)_2$ (10 s, P*K*α), scapolite (15 s, Cl*K*α), orthoclase (10 s, K*K*α), diopside (10 s, Ca*K*α), $MnTiO_3$ (10 s, Ti*K*α), $MnTiO_3$ (10 s, Mn*K*α), hematite (10 s, Fe*K*α), sphalerite (15 s, Zn*K*α), and barite (10 s, Ba*L*α).

Identification of minerals not analyzed with WDS was confirmed by taking an element scan using energy-dispersive spectroscopy at the University of Maine.

Crystal structure

Chopinite and sarcopside are of the olivine structure type, but with ordered vacancies and strongly distorted octahedra due to the valence 5+ for P (Fig. 1). In olivine each oxygen atom is coordinated to 3 M and 1 Si yielding the "ideal" bond strength of 2 for oxygen (3 x 2/6 + 4/4). In sarcopside O1, O2, and O3 (our numbering) are bonded 2× to M and 1× to P yielding 2 × 2/6 + 5/4 = 1.917 indicating slight underbonding. However, O4 bonds 3 × to M and 1 × to P yielding 3 × 2/6 + 5/4 = 2.25 indicating significant overbonding. For this reason all M-O4 and P-O4 bonds are rather long (Table 5), which results in strong distortions and a marked ordering of Mg at the M2 site (89 % Mg). Fe^{2+} is ordered at M1 (52 % Fe), most likely because of axial symmetry of the M1 octahedron, that is, the presence of three 180° O-M1-O angles (Table 5). This symmetry seems to be more appropriate for arrangement of *d*-electron orbitals than the M2 octahedron, which lacks this axial symmetry (with 152°, 153°, and 169°). The M1 octahedron

Table 3. Anisotropic displacement parameters U_{ij} with standard deviations in parentheses for chopinite.

Site	U_{11}	U_{22}	U_{33}	U_{12}	U_{13}	U_{23}
Fe1	0.0126(4)	0.0065(4)	0.0103(4)	–0.0006(3)	0.0024(3)	0.0001(3)
Mg2	0.0093(5)	0.0088(5)	0.0086(4)	–0.0001(3)	0.0009(4)	0.0001(3)
P	0.0112(3)	0.0078(3)	0.0099(3)	0.0000(3)	0.0005(3)	–0.0002(3)
O1	0.013(1)	0.009(1)	0.012(1)	0.0009(8)	0.0014(8)	–0.0007(7)
O2	0.014(1)	0.0115(9)	0.0101(9)	–0.0010(8)	–0.0003(9)	–0.0002(7)
O3	0.011(1)	0.011(1)	0.015(1)	–0.0008(8)	0.0033(7)	–0.0019(8)
O4	0.013(1)	0.0096(9)	0.014(1)	0.0000(8)	0.0003(8)	–0.0014(7)

Table 4. Atomic coordinates and isotropic displacement parameters, with standard deviations in parentheses, for chopinite.

site	x/*a*	y/*b*	z/*c*	B_{eq} (Å^2)	Occupancy
Fe1	1/2	0	1/2	0.77(1)	0.518(6)
Mg1	1/2	0	1/2	0.77(1)	0.482
Fe2	0.2377(2)	0.0118(1)	0.77910(8)	0.70(1)	0.107(4)
Mg2	0.2377(2)	0.0118(1)	0.77910(8)	0.70(1)	0.893
P	0.2562(1)	–0.4293(2)	0.59884(6)	0.76(1)	1
O1	0.2756(3)	0.2519(4)	0.6058(2)	0.89(3)	1
O2	0.2552(3)	–0.3189(4)	0.4588(2)	0.92(3)	1
O3	0.0612(3)	–0.3153(4)	0.6789(2)	0.97(3)	1
O4	0.5334(3)	0.2781(4)	0.3373(2)	0.95(3)	1

Anisotropically refined atoms are given in the form of the isotropic equivalent displacement parameter defined as $B_{eq} = (8/3)\ \pi^2\ \Sigma i(\Sigma j(\ Uij\ ai^*\ aj^*\ ai.aj))$

Table 5. Bond lengths (Å) and angles (°).

	Length	Angles				
Fe1						
O1_$1	2.102(2)					
O1	2.102(2)	180				
O2_$1	2.139(2)	94.25(7)	85.75(7)			
O2	2.139(2)	85.75(7)	94.25(7)	180.00(7)		
O4	2.140(2)	83.41(7)	96.59(7)	69.30(7)	110.70(7)	
O4_$1	2.141(2)	96.59(7)	83.40(7)	110.70(7)	69.30(7)	180
Mean	2.127	O1_$1	O1	O2_$1	O2	O4
Vacancy						
O2	2.187(2)					
O2_$5	2.187(2)	180.00(7)				
O1_$5	2.289(2)	92.10(6)	87.90(6)			
O1	2.289(2)	87.90(6)	92.10(6)	180		
O3_$5	2.394(2)	112.67(7)	67.33(7)	82.17(6)	97.83(6)	
O3	2.394(2)	67.33(7)	112.67(7)	97.83(6)	82.17(6)	180
Mean	2.290	O2	O2_$5	O1_$5	O1	O3_$5
Mg2						
O3_$4	2.006(2)					
O2_$3	2.061(2)	91.50(9)				
O4_$5	2.100(2)	118.74(9)	85.66(8)			
O1	2.127(2)	93.52(8)	169.11(9)	83.45(8)		
O3	2.133(2)	88.45(6)	97.21(8)	152.66(8)	92.59(8)	
O4_$1	2.282(2)	153.24(9)	100.06(8)	86.38(5)	79.52(7)	66.32(7)
Mean	2.118	O3_$4	O2_$3	O4_$5	O1	O3
P						
O1_$2	1.523(2)					
O3	1.526(2)	112.74(11)				
O2	1.529(2)	112.70(11)	112.85(12)			
O4_$1	1.576(2)	112.11(11)	102.43(10)	103.15(11)		
Mean	1.539	O1_$2	O3	O2		

Symmetry codes. $1: –x+1,–y,–z+1. $2: x, y–1, z. $3: x, –y–1/2, z+1/2. $4: –x, y+1/2, –z+3/2. $5: x, –y+1/2, z+1/2.

is slightly larger (<M1-O> = 2.217 Å) than M2 (<M2-O> = 2.118 Å). In addition, M1 is more regular: the difference between the largest and shortest M-O bond is 0.038 Å for M1 but 0.274 Å for M2. Lastly, M1 is adjacent to the vacant octahedral site, thus the M1 octahedron is freer to adopt a favorable coordination for Fe^{2+}.

The largest octahedral site (<M-O> = 2.290 Å) in the structure is M1', which is vacant in sarcopside and chopinite. Local occupation of M1' would increase the bond strength of O1, O2, and O3 by additional 2/6, which is energetically not favorable. Nevertheless, the highest positive peak in the final difference-Fourier map of 0.4 e/Å^3 was found at M1'. This residual density was not considered in the refinement because the highest negative peak close to the tetrahedral P sites was also –0.4 e/Å^3. One may speculate that the minor substitution of P^{5+} by Si^{4+} determined by electron microbe-analyses (Table 6) is charge balanced by very minor occupation of M1' by additional Mg or Fe.

There is a minor difference between X_{Mg} obtained from the structure refinement (X_{Mg} = 0.756) *vs.* the corresponding value (X_{Mg} = 0.720) determined by electron microprobe analyses (Table 6). There are several possible explanations for this discrepancy. (1) X-ray single-crystal diffraction yields the 3-dimensional average bulk composition of the entire crystal, whereas the electron-microprobe beam does not penetrate very far below the surface of the section, *i.e.*, the different results could be due to compositional zoning. (2) Because Fe is the atom with the strongest scattering power in the structure, there is also a minor correlation in the structure refinement between Fe occupancy on one hand, scale factor and displacement parameters on the other. (3) The very minor (0.4 e/Å^3) residual density at M1' was not considered. Furthermore, the twinning model with {100} as twin plane maps M1 on M1' (Fig. 1). Thus there is some correlation between M1' occupancy and the twinning contribution. Another possible explanation is the ionization level of oxygen. However, Armbruster *et al.* (1990) tested the effect of choosing neutral *vs.* ionic scattering factors on displacement parameters (Beq), which are even more sensitive than occupancies, and found no significant variation in B_{eq} of T sites in models with Si^{4+} and Al^{+3} compared to those with neutral Si and Al in albite.

The synthetic analogue $Mg_3(PO_4)_2$ of chopinite was first synthesized by Berthet *et al.* (1972) as a metastable product of the following solid state reaction at 660°C: 2×LiMg(PO_4) (olivine structure-type) + $MgSO_4$ → $Mg_3(PO_4)_2$ (sarcopside structure-type) + Li_2SO_4. The above authors determined from X-ray powder data the correct symmetry ($P2_1/b$;

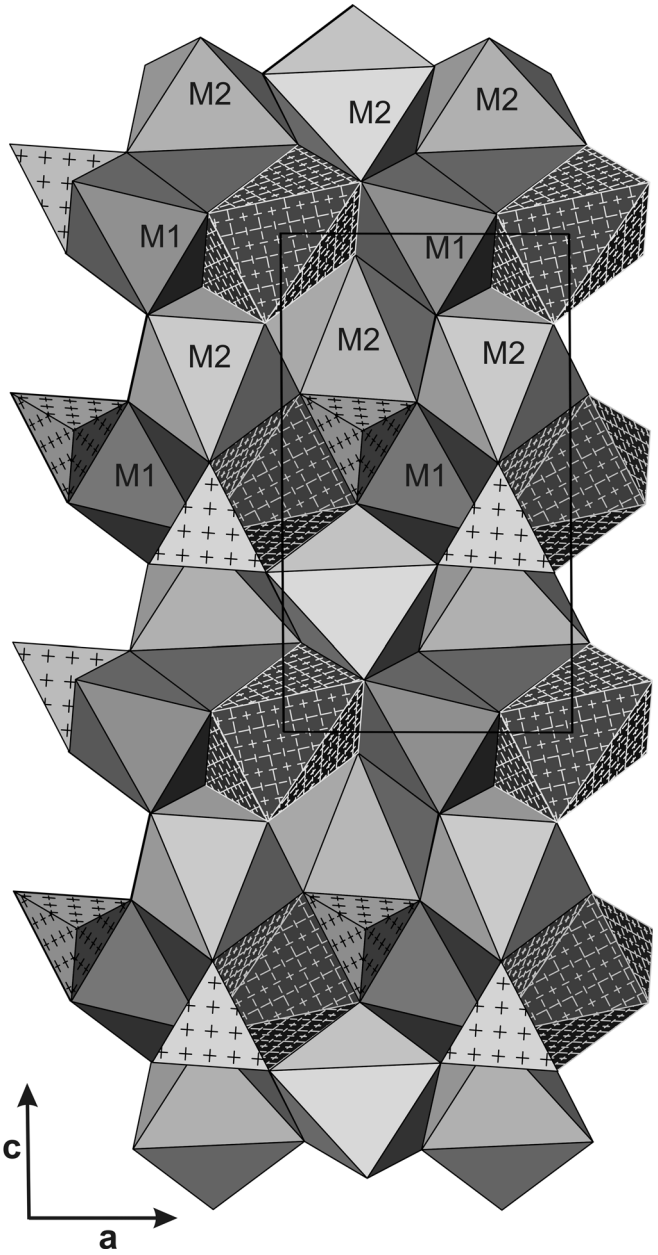

Fig. 1. Projection of the chopinite structure along **b**. M2 octahedra (Mg enriched) form unbroken edge-sharing chains parallel to **a**, whereas M1 octahedra (Fe enriched) alternate with vacant polyhedra (dark with line and cross pattern). PO_4 tetrahedra are marked with crosses.

their setting: a = 5.912(2), b = 10.21(3), c = 4.73(2), Å, $\gamma = 90°60'$) and derived in analogy to olivine a correct structure model with ordered octahedral vacancies. At 820°C this metastable chopinite analogue transformed to $Mg_3(PO_4)_2$ having the farringtonite structure. Farringtonite is not based on a hexagonal closest-package of oxygen (as the olivine and sarcopside structure-type) and has for this reason also a larger unit-cell volume, 316.6 Å^3 (Nord & Kierkegaard, 1968) *vs.* 285.8 Å^3. In farringtonite Mg occurs in fivefold and octahedral coordination.

Recently Henry *et al.* (2003) refined the sarcopside-like structure of synthetic $Fe_2Ni(PO_4)_2$ by neutron powder diffraction and found Fe enriched at M2 and Ni dominating at M1. This Fe order scheme is the opposite of that found in chopinite. However, in $Fe_2Ni(PO_4)_2$ two transition metal ions are competing with each other for the most favorable coordination. In this case Ni occupies the less distorted site. Previous crystallographic studies of solid solutions of $Me_3(PO_4)_2$ with Me = Co^{2+}, Mg, Zn, Mn^{2+}, Fe^{2+} in sarcopside-like $Ni_3(PO_4)_2$ yielded the preference Ni > Co >Mg, Zn > Mn >> Fe for M1 over M2 (Nord, 1984). A neutron powder structure-refinement of synthetic sarcopside $Fe_3(PO_4)_2$ at 59 K (Warner *et al.*, 1992) yielded <M1-O> = 2.147 Å and <M2-O> = 2.159 Å, whereas a single-crystal X-ray structure refinement (Moore, 1972) of natural $(Fe_{0.78}Mn_{0.21}Mg_{0.01})_3(PO_4)_2$ sarcopside gave <M1-O> = 2.130 Å and <M2-O> = 2.164 Å. Due to the similarity of Mn and Fe scattering factors for X-rays Moore (1972) did not determine whether Fe and Mn order in sarcopside, but instead assumed equal distribution of both elements at M1 and M2. However, comparison of <M1-O> and <M2-O> bond lengths with those of Warner *et al.* (1992) suggests that the larger Mn^{2+} will order at M2.

Physical and optical properties of chopinite

Most physical properties cannot be determined because of the small grain size and the very limited amount of available material. Two good cleavages are evident in photomicrographs and back scattered electron images (see below); these could {001} and {100}, the two good cleavages reported for sarcopside (Hurlbut, 1965). Density calculated with empirical formula is 3.34 g/cm^3.

Chopinite is colorless and transparent, biaxial (–), α 1.595(2), β 1.648(2), γ 1.656(2) (589 nm). $2V_x$ (meas.) = 40(2)°, $2V_x$ (calc.) = 41°. Dispersion was not visible, but the interference figure was poor due to inclusions of brownish material. Assuming that the twin plane is {100}, orientation of the principal vibration directions derived from stereographic projection is X // b, Z /\ a ~55°. Larsen & Berman (1934) reported Z // b, X /\ c = 45° for sarcopside, but they gave the cleavages as perfect in {010} and {100}. Hurlbut (1965) was unable to confirm the Larsen & Berman orientation and reported an apparent optical orientation for sarcopside characteristic of a triclinic crystal with Y closest to b. Hurlbut (1965) failed to resolve the obvious (to him) inconsistency with Larsen & Berman (1934), and we have no explanation why the orientation for chopinite differs from both of those reported for sarcopside.

Chemical composition and compatibility index of chopinite

The three analyzed chopinite grains are fairly homogeneous and virtually identical in composition (Table 6). Chopinite is nearly pure ferromagnesian phosphate containing but minor Ca, Mn and Si. We did not analyze Li, which was reported in sarcopside (Hurlbut, 1965) and is an essential constituent of the structurally related triphylite-lithiophyllite series. Fluorine contents obtained at University of Maine are negligible,

Table 6. Analyses of chopinite in section 121401E4-1.

Grain	1	1	2	2	3*	3*
Probe	UM	Cam	UM	Cam	UM	SREF
No. spots	12	7	16	5	11	
wt%						
SiO_2	0.13(4)	0.10(3)	0.23(6)	0.16(4)	0.32(3)	
P_2O_5	48.00(50)	47.80(49)	47.84(53)	47.54(17)	47.32(44)	49.64
TiO_2	b.d.	0.01(2)	b.d.	0.01(2)	b.d.	
Al_2O_3	0.02(3)	0.02(4)	0.01(2)	0.01(2)	0.05(4)	
MgO	30.85(25)	30.29(42)	30.87(31)	29.92(50)	30.35(41)	31.96
MnO	0.11(4)	0.14(6)	0.14(4)	0.11(4)	0.15(3)	
FeO	20.75(32)	20.34(42)	21.11(38)	20.53(45)	20.99(38)	18.40
ZnO	n.a	0.03(6)	n.a	0.05(6)	n.a	
Na_2O	0.01(4)	b.d.	0.01(4)	0.01(2)	b.d.	
K_2O	n.a	0.01(1)	n.a	b.d.	n.a	
CaO	0.11(10)	0.02(2)	0.10(10)	0.03(2)	0.35(17)	
BaO	n.a	0.11(18)	n.a	0.02(3)	n.a	
F	0.04(6)	0.19(30)	0.01(11)	0.18(33)	0.02(4)	
Cl	b.d.	b.d.	b.d.	0.01(1)	0.01(2)	
Sum	99.99	98.88	100.30	98.41	99.54	100.00
Formulae per 8 Oxygen						
Si	0.006	0.005	0.011	0.008	0.016	
P	1.965	1.977	1.956	1.976	1.952	2.0000
Al	0.001	0.001	0.001	0.001	0.003	
Mg	2.224	2.206	2.223	2.190	2.204	2.2675
Mn	0.005	0.006	0.006	0.005	0.006	
Fe	0.839	0.831	0.853	0.843	0.855	0.7325
Zn	–	0.001	–	0.002	–	
Na	0.001	0.000	0.001	0.001	0.000	
Ca	0.006	0.001	0.005	0.001	0.018	
Sum	5.046	5.029	5.055	5.028	5.055	5.000
X_{Mg}	0.726	0.726	0.723	0.722	0.720	0.756

Notes: Probe: UM – University of Maine, Cam – Camparis, SREF – single-crystal structure refinement. n.a. – not analyzed; b.d. – below detection. All Fe as FeO. Numbers in parentheses are 1σ standard deviations of last 1 or 2 digits in the averages. Totals does not include F, Cl. Formulae do not include Ba, F or Cl. X_{Mg} = atomic Mg/(Mg+Fe). * Grain used for optical and crystallographic studies.

whereas those obtained at the Centre de Microanalyse Camparis vary with the standard used, ranging from below detection to 0.10 wt% with the topaz standard and from 0.62 to 0.76 wt% with the fluorapatite standard. Averages of individual grains in Table 6 include measurements with both F standards, resulting in high standard deviations for F. Analyses at the two laboratories gave virtually identical formulae, except the Centre de Microanalyse Camparis analyses gave a closer approach to ideal stoichiometry in terms of (P+Si):(Mg+Fe+Mn+Ca) ratio and lower Ca contents. Both sets of analyses gave a significantly lower Mg:(Fe+Mn) ratio than the crystal structure refinement (see above).

The Gladstone – Dale relation (Mandarino, 1981) gives a compatibility index $1 - (K_P/K_C) = 0.001$ (superior) for grain no. 3.

Relationship of chopinite to other (Mg, Fe, Mn)$_3$(PO$_4$)$_2$ phases

Only two terrestrial minerals are composed almost exclusively of (Mg, Fe, Mn)$_3$(PO$_4$)$_2$: the isostructural phases chopinite and sarcopside (Fig. 2). Graftonite (Fe > Mn) and beusite (Mn > Fe) are (Fe, Mn, Ca, Mg)$_3$(PO$_4$)$_2$ phosphates containing significant Ca. Graftonite has a higher Mn/Fe ratio and lower Mg/Fe ratio than associated sarcopside. The Brattnevet chopinite is far more magnesian than any known sarcopside or graftonite, and unlike most terrestrial sarcopside, it is not intergrown with either graftonite or triphylite. Experiments suggest that there is no break in solid solution between synthetic end-member chopinite and sarcopside (*e.g.* Annersten & Nord, 1980; Charalampides *et al.*, 1988). An Mg-dominant analogue of graftonite has not been reported in nature or experiment.

Meteoritic Mg-Fe-Mn phosphates include not only graftonite and sarcopside, but also farringtonite (Fig. 2). Synthetics with the farringtonite structure extend to 60% Fe-end-member (Annersten *et al.*, 1980). Graftonite and sarcopside in IVA and IIIAB irons are Fe-Mn solid solutions containing negligible Mg; graftonite is richer in Mn than associated sarcopside; identification by X-ray diffraction was possible in a few cases (Bild, 1974; Olsen *et al.*, 1999). In contrast, phosphates in the Graves Nunatak (GRA) 95209 lodranite are Mn-poor (Mg, Fe)$_3$(PO$_4$)$_2$ phases that range from Mg-rich to Fe-rich, referred to as "farringtonite" and "Mg-graftonite" or "graftonite/sarcopside", respectively

(Floss, 1999; McCoy *et al.*, 2006). A Fe-Mg phosphate in the Brahin pallasite also has the stoichiometry of sarcopside (Buseck & Holdsworth, 1977). Although information other than chemical was not obtained to identify these ferromagnesian phosphates, there is reason to suspect that two or three phases are present in GRA 95209 (see below).

Occurrence and associated minerals

Chopinite occurs in one (Fig. 3) of many fluorapatite segregations in a quartz mass roughly 10 cm thick and 3 m long in biotite-quartz-plagioclase paragneiss, which also contains segregations of prismatine and cordierite at this locality on

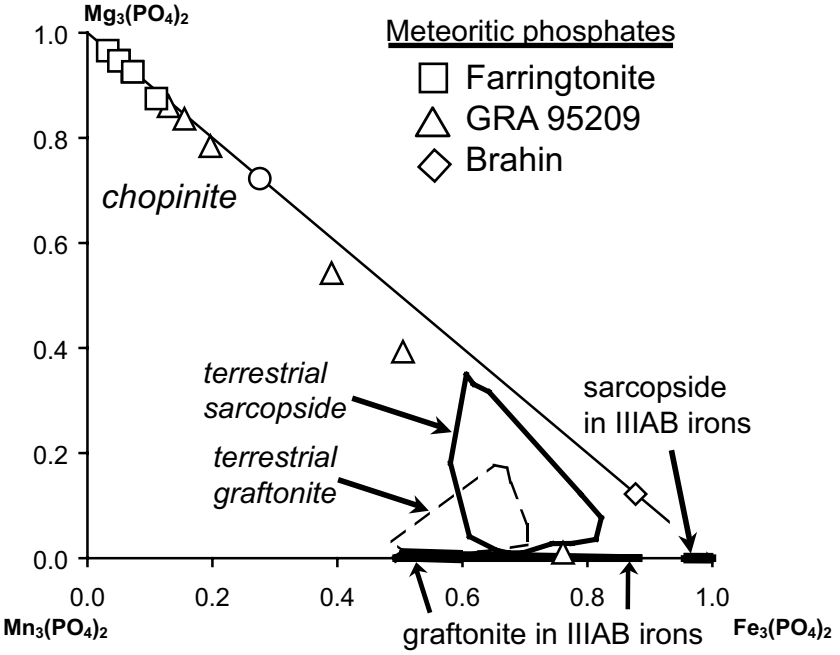

Fig. 2. Plot of natural farringtonite, graftonite, sarcopside, and chopinite compositions in terms of the divalent cations excluding Ca. The fields for terrestrial graftonite (dashed line) and sarcopside (solid line) are largely from intergrowths (Černý *et al.,* 1998; Corbella i Cordomí & Melgarejo i Draper, 1990; Fontan & Fransolet, 1986; Fransolet, 1977; Fransolet *et al.*, 1986; Hurlbut, 1965; Huvelin *et al.* (1971); Lindberg (1950); Livingstone, 1980; Malló *et al.*, 1995; Palache *et al.* (1951); Povondra *et al.*, 1987; Roda *et al.*, 2004; Smeds *et al.*,1998; Stalder & Rozendaal, 2002; Zhang, 1995). Sources of other data: chopinite (this paper); farringtonite (Fuchs *et al.*, 1973; Bild, 1974; Buseck & Holdsworth, 1977); phosphates in meteorite GRA 95209 (Floss, 1999; McCoy *et al.*, 2006); graftonite and sarcopside in IVA and IIIAB iron meteorites (Bild, 1974; Olsen *et al.*, 1999); phosphate (sarcopside?) in the Brahin pallasite (Buseck & Holdsworth, 1977).

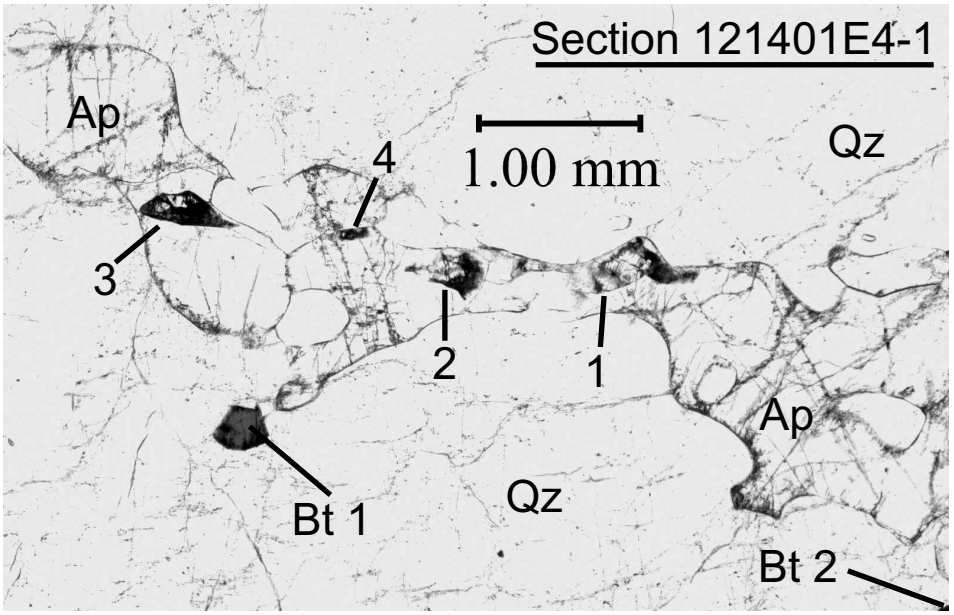

Fig. 3. Photomicrograph of fluorapatite segregation (Ap) containing four grains of chopinite (numbered, Fig. 4) in section 121401E4. Matrix is quartz (Qz); Bt 1 and 2 – biotite grains closest to chopinite (Table 9); only a tip of the second grain is visible in this photograph. Plane polarized light.

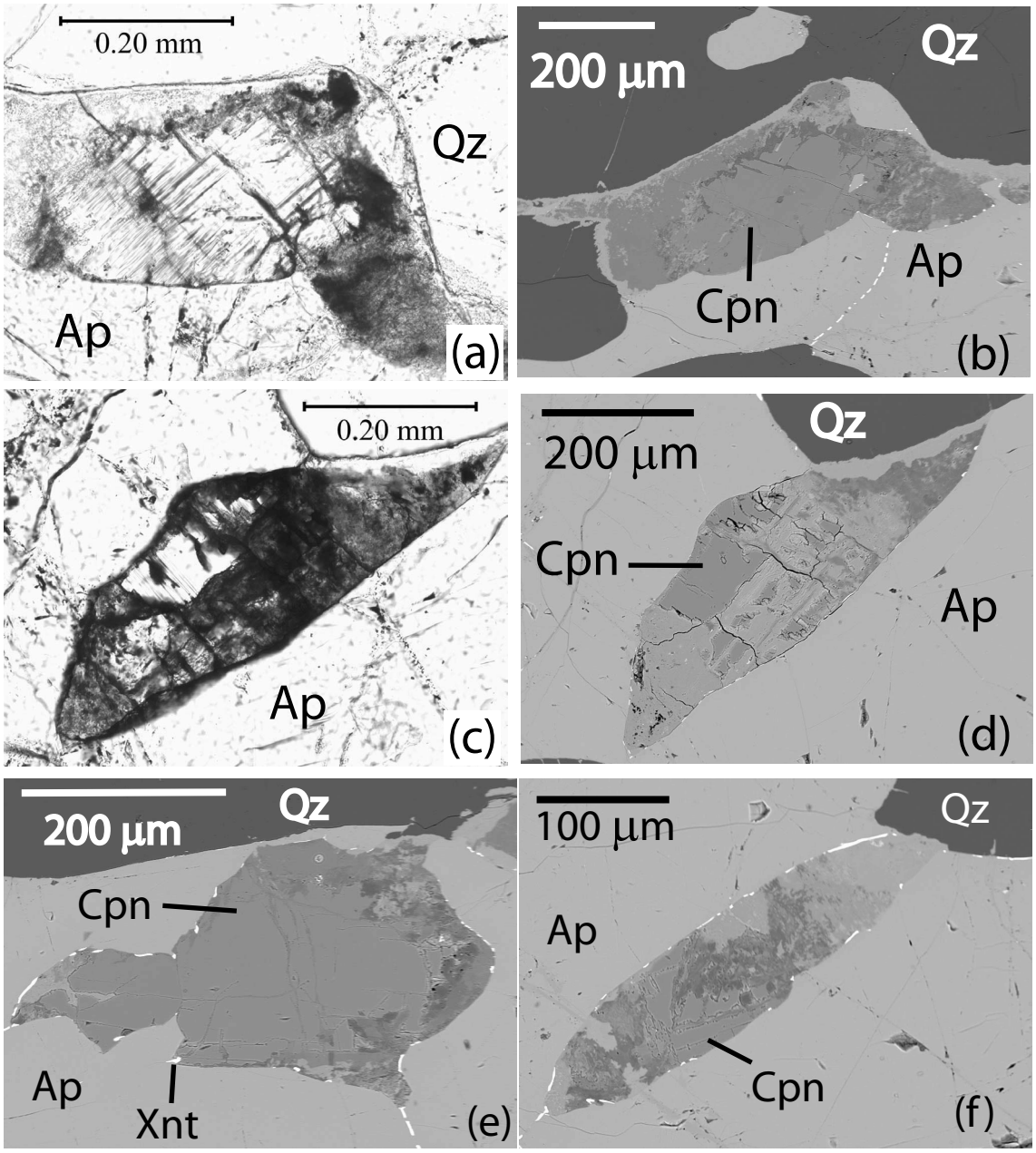

Fig. 4. Chopinite (Cpn) enclosed in fluorapatite (Ap) in section 121401E4. (a) Photomicrograph of grain 1. Plane polarized light. (b) Back scattered electron image of this grain. (c) Photomicrograph of grain 3. Plane polarized light. (d) Back scattered electron image of this grain. (e) Back scattered electron image of grain 2. (f) Back scattered electron image of grain 4. Qz – quartz, Xnt – xenotime-(Y). Darker areas in the photomicrographs are secondary minerals.

Brattnevet Peninsula. The segregation is 8 mm long, variable in thickness and highly irregular in outline (only a portion is shown in Fig. 3). Overall, 31 sections were cut from 22 different slices of sample 121401E, but only one section contained chopinite, four grains in all (section 121401E4). These grains are anhedral, or show some roughly planar surfaces, and range from 0.1 × 0.3 mm to 0.2 × 0.6 mm (Fig. 4). The mineral is partially altered and its original form is obscured; the present grains could have been aggregates of two or three single crystals. Cores of unaltered material range from less than 0.1 × 0.1 mm to 0.2 × 0.4 mm and constitute single crystals, albeit one crystal appears to have been broken. Alteration of chopinite resulted in a mixture of phosphates, including secondary fluorapatite, a phase similar to the isokite-like mineral reported by Grew *et al.* (2007), and xenotime-(Y), the last in specks (<10 μm) along grain boundaries (Fig. 4e). Other secondary phases appear green or brown in thin section, but could not be identified. No unaltered chopinite is in contact with quartz, but altered chopinite contacts quartz at one spot (Fig. 4f).

Wagnerite-*Ma5bc*, biotite, albite, pyrite, and monazite-(Ce) are also present in the chopinite-bearing section, but none contacts chopinite. Overall, a diverse suite of minerals was found in specimen 121401E, but many very sparingly

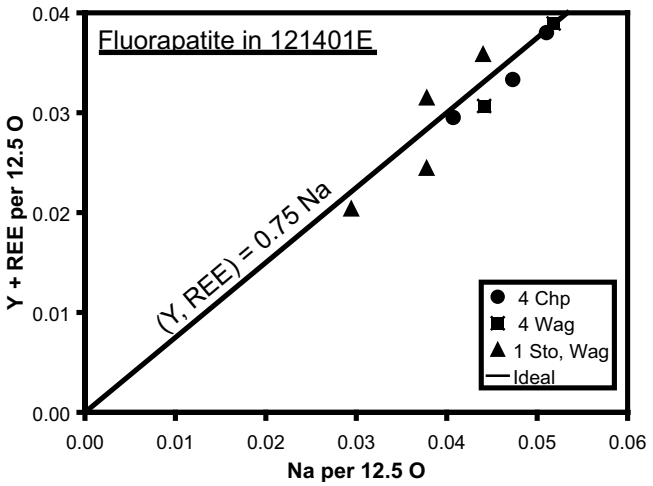

Fig. 5. Plot of fluorapatite Na, Y and total rare earth element (REE) contents in specimen 121401E, including data from Grew *et al.* (2006). Legend gives section number and identity of nearby ferromagnesian phosphate mineral (abbreviations in Table 7). Line is for reference only.

Table 7. Minerals and their occurrence in specimen 121401E.

Mineral	Ap seg*	Qz matrix
Phosphates		
Fluorapatite (Ap)	XX	XX
Wagnerite (Wag)	X	–
Stornesite-(Y) (Sto)	T	–
Chopinite (Chp)	R	–
Monazite-(Ce) (Mnz)	T	–
Xenotime-(Y) (Xnt)	T	–
"Souzalite-like"	2nd	–
Silicates		
Quartz (Qz)	X	XX
Plagioclase (Pl)	X	X
K-feldspar (Kfs)	x	–
Sillimanite (Sil)	T	T
Orthopyroxene (Opx)	–	R
Sapphirine (Spr)	–	R
Biotite (Bt)	X	X
Chlorite	2nd	2nd
Sericite	2nd	2nd
Zircon (Zrn)	–	R
Oxides		
Hercynite (Hc)	x	T
Corundum (Crn)	–	R
Rutile (Rt)	–	R
Magnetite (Mgt)	x	T
Ilmenite (Ilm)**	x	T
Miscellaneous		
Pyrite	T	–
Celestine	R	–
Fe carbonate	2nd	–

Note: XX – very abundant; X – abundant throughout; x – present throughout; T – in trace amounts; R – rare, *i.e.*, <5 grains total in 1 or 2 sections; 2^{nd} – a secondary phase, generally sparse. *In the fluorapatite segregations, with or without quartz, in contrast to minerals not found within the segregations. **Includes exsolved hematite and secondary "pseudorutile".

(Table 7). The phosphates occur exclusively as inclusions in apatite, although contacts with quartz are common; in a few cases, wagnerite is found between apatite and silicates.

The coarse-grained fluorapatite hosting chopinite and wagnerite in section 121401E4 is relatively rich in Mg, Cl, Fe and Y (Table 8), features characteristic of fluorapatite in stornesite-(Y)-bearing sections of 121401E and of specimens from the type locality (Grew *et al.,* 2006). Yttrium and total rare earth elements (REE) increase regularly with Na in sample 121401E, but not at the ratio predicted by the substitution (Y, REE) + Na = 2Ca (Fig. 5). Halogen contents of apatite vary little from spot to spot (Fig. 6a).

Next to fluorapatite, the most abundant phosphate is wagnerite. Two inclusions of partially altered pale-yellow wagnerite, up to 1.5 mm long, in a second, larger apatite segregation in the chopinite-bearing thin section 121401E4 are 5*b* polytype and contain little Ti (Table 8). Two other grains in this section average 0.33 wt% TiO_2 and X_{Mg} = 0.92. In other sections of 121401E wagnerite is commonly developed around K-feldspar or biotite and its break down products.

Brown flakes of Ti-rich biotite (Table 9) are commonly enclosed in fluorapatite or in quartz near fluorapatite (*e.g.* Fig. 3). Cl/(Cl+F) ratio (Fig. 6b) and Ti content vary inversely with X_{Mg}. Distributions of Cl, F and OH between biotite and apatite can be used as geothermometers (Zhu & Sverjensky, 1992), which we applied to the data obtained on the U Maine electron microprobe assuming a constant apatite X_{Cl} throughout sample 121401E (Fig. 6a) and P = 6 kbar. Chlorine distribution [ln K_D = 4.35 – 4.95, where $K_D = (Cl/OH)_{Ap}/(Cl/OH)_{Bt}$] gives less than 500 °C, whereas F distribution [ln K_D = 3.32 – 4.02] gives 698–788 °C (cf. 800–860 °C for the metamorphic peak, Grew *et al*., 2006).

Perthitic K-feldspar occurs as selvages formed from breakdown of biotite (Grew *et al*., 2006) and as coarser grains enclosing oriented vermicules and rounded blebs of quartz (Fig. 7). P_2O_5 contents of K-feldspar and plagioclase (An9-18) enclosed in fluorapatite or contiguous to fluorapatite range from 0.09 to 0.51 wt% (Grew *et al.*, 2006; this paper, Table 10). Albite (An0.3) is a minor component of the quartz matrix in the chopinite-bearing section.

Orthopyroxene is largely altered to phyllosilicates; it is separated from apatite and from small grains of wagnerite enclosed in apatite by a quartz-K-feldspar-oligoclase corona (Fig. 8a; Table 11). Sapphirine is found in direct contact with quartz (Fig. 8b) or enclosed in sillimanite, which isolates it from fluorapatite and quartz. In most cases, sillimanite appears to be a later-formed mineral, being found with the low-Ti skeletal biotite and as an overgrowth on corundum (Fig. 8c,d; Table 11); a prism is also enclosed in fluorapatite.

Hercynite (Table 12), magnetite (Table 12) and ilmenite are found both as vermicules and tiny grains (several tens micrometers) in K-feldspar resulting from breakdown of biotite enclosed in fluorapatite, and as very rare independent coarser grains several hundreds micrometers across in quartz, either enclosed in the fluorapatite segregations or in the quartz matrix. In contrast, corundum (Table 11) has only been found in quartz, from which it is separated by a thin

Table 8. Selected analyses of fluorapatite (Ap) and wagnerite-*Ma5bc* (Wag) in the chopinite-bearing section 121401E4-1.

Mineral	Ap	Ap	Ap	Wag*	Wag**
Grain	1^0	2^0	5^0	4	5
No. spots	10	17	18	13	20
wt%					
SiO_2	b.d.	b.d.	b.d.	0.02	0.03
P_2O_5	42.02	41.98	41.44	41.90	42.10
SO_3	b.d.	b.d.	0.01	n.a.	n.a.
TiO_2	b.d.	b.d.	b.d.	0.08	0.09
Al_2O_3	0.03	b.d.	b.d.	b.d.	0.01
MgO	0.69	0.86	0.61	45.42	45.28
MnO	0.22	0.27	0.29	0.12	0.14
FeO	2.44	2.74	3.10	6.69	6.68
Na_2O	0.31	0.29	0.31	b.d.	b.d.
CaO	50.43	50.27	49.88	0.13	0.11
SrO	0.03	0.02	b.d.	n.a.	n.a.
Y_2O_3	0.56	0.47	0.55	n.a.	n.a.
La_2O_3	0.10	0.07	0.10	n.a.	n.a.
Ce_2O_3	0.24	0.21	0.29	n.a.	n.a.
Nd_2O_3	0.06	0.06	b.d.	n.a.	n.a.
Yb_2O_3	0.01	0.06	0.06	n.a.	n.a.
UO_2	0.08	0.04	b.d.	n.a.	n.a.
F	2.37	2.28	2.36	10.65	10.75
Cl	2.09	2.10	2.07	b.d.	b.d.
H_2O calc	0.10	0.14	0.09	0.32	0.29
O=F, Cl	–1.47	–1.43	–1.47	–4.48	–4.53
Sum	100.32	100.43	99.71	100.87	100.95
Formulae					
O (anhyd.)	12.5	12.5	12.5	4.5	4.5
Si	0	0	0	0.001	0.001
P	3.019	3.014	3.005	0.983	0.986
S	0	0	0.001	–	–
Ti	0.000	0	0.000	0.002	0.002
Al	0.003	0	0.000	0	0.000
Mg	0.087	0.109	0.078	1.876	1.868
Mn	0.016	0.020	0.021	0.003	0.003
Fe	0.173	0.194	0.222	0.155	0.155
Na	0.051	0.047	0.052	–	–
Ca	4.585	4.567	4.578	0.004	0.003
Sr	0.001	0.001	0.000	–	–
Y	0.025	0.021	0.025	–	–
La	0.003	0.002	0.003	–	–
Ce	0.008	0.007	0.009	–	–
Nd	0.002	0.002	0.000	–	–
Yb	0	0.001	0.001	–	–
U	0.002	0.001	0.000	–	–
Sum	7.975	7.986	7.997	3.023	3.018
F	0.637	0.613	0.640	0.933	0.940
Cl	0.300	0.302	0.300	0	0
H_{calc}	0.063	0.086	0.059	0.067	0.060
Sum	1.000	1.000	1.000	1	1
X_{Mg}	0.335	0.360	0.259	0.924	0.924

Notes: n.a. – not analyzed; b.d. – below detection. All Fe as FeO. H_2O calculated from stoichiometry: F + Cl + H = 1. X_{Mg} = atomic Mg/(Mg+Fe).
Analyses done at the University of Maine.
^{0}Near to chopinite grains 1 and 2, wagnerite grain 5, respectively
*a = 9.670(3), b = 31.74(1), c = 11.924(4) Å, β = 108.25(2)°, V = 3481(2) Å^3
**a = 9.681(3), b = 31.685(8), c = 11.919(3) Å, β = 108.14(2)°, V = 3474(2) Å^3

selvage of sillimanite (*e.g.* Fig. 8c,d, Table 11). A rutile grain (Table 12) occurs with zircon along the boundary of quartz with a sillimanite aggregate enclosing corundum. Temperatures calculated from the 386 ppm Zr measured in rutile are 751 °C (calibration of Zack *et al.,* 2004) and 663 °C (calibration of Watson *et al.*, 2006).

Origin of chopinite

Chopinite is distinct from sarcopside not only in the dominance of Mg over Fe, but also in being found as discrete grains enclosed in fluorapatite in a metamorphic assemblage. There are few terrestrial occurrences of sarcopside that is not intergrown with graftonite or triphylite (*e.g.*

Table 9. Selected analyses of biotite in sample 121401E.

Sect / gr	4-2 / 1	4-3 / 1	19 / 2	4-1 / 1°	4-1 /2°
Probe	UM	UM	UM	Cam	Cam
F std	Pol	Pol	Pol	Ap	Ap
No. spots	10	10	7	2	2*
wt%					
SiO_2	37.08	36.64	36.92	37.03	37.22
P_2O_5	0.04	0.07	0.03	0.03	0.04
TiO_2	5.07	6.19	5.58	5.37	5.43
Al_2O_3	15.18	15.09	14.83	16.07	15.59
Cr_2O_3	0.15	0.09	0.10	n.a.	n.a.
K_2O	9.63	9.58	9.58	9.81	9.67
Na_2O	0.10	0.08	0.17	0.10	0.12
CaO	b.d.	0.02	b.d.	0.01	0.01
BaO	0.13	0.11	0.07	b.d.	b.d.
MgO	14.10	12.03	13.09	14.08	14.71
MnO	0.02	0.04	b.d.	0.01	0.03
FeO	14.63	16.47	16.12	12.78	13.09
ZnO	n.a.	n.a.	n.a.	b.d.	0.09
F	1.32	1.10	1.46	0.92	0.82
Cl	0.41	0.52	0.60	0.44	0.37
H_2O calc	3.32	3.36	3.19	3.51	3.59
O=F, Cl	–0.65	–0.58	–0.75	–0.48	–0.43
Total	100.52	100.83	101.01	99.67	100.34
Formula per 22 O anhydrous					
Si	5.495	5.464	5.490	5.480	5.477
P	0.005	0.009	0.004	0.004	0.005
^{IV}Al	2.500	2.527	2.506	2.516	2.518
Sum IV	8.000	8.000	8.000	8.000	8.000
Ti	0.565	0.694	0.625	0.598	0.601
^{VI}Al	0.152	0.125	0.093	0.286	0.186
Cr	0.018	0.011	0.012	–	–
Mg	3.116	2.675	2.902	3.107	3.227
Mn	0.002	0.005	0.000	0.001	0.003
Fe	1.813	2.054	2.005	1.582	1.610
Zn	–	–	–	0.000	0.010
Sum VI	5.666	5.564	5.637	5.573	5.637
K	1.820	1.823	1.818	1.852	1.815
Na	0.028	0.023	0.049	0.029	0.033
Ca	0.000	0.004	0.000	0.001	0.001
Ba	0.007	0.007	0.004	0.000	0.000
Sum XII	1.856	1.857	1.870	1.882	1.849
Total	15.522	15.420	15.507	15.455	15.486
F	0.619	0.521	0.685	0.429	0.382
Cl	0.103	0.132	0.152	0.109	0.091
H_{calc}	3.278	3.347	3.163	3.461	3.527
Sum	4.000	4.000	4.000	4.000	4.000
X_{Mg}	0.632	0.566	0.591	0.663	0.667

Notes: Sect/gr – section/grain. Probe: UM – University of Maine, Cam – Camparis. n.a. – not analyzed; b.d. – below detection. F standards: Pol – polylithionite, Ap – fluorapatite. All Fe as FeO. H_2O calculated from stoichiometry: F + Cl + H = 4. X_{Mg} = atomic Mg/(Mg+Fe). °Grains 1 and 2 are the closest biotite grains to chopinite (Fig. 3). *Only one spot for F.

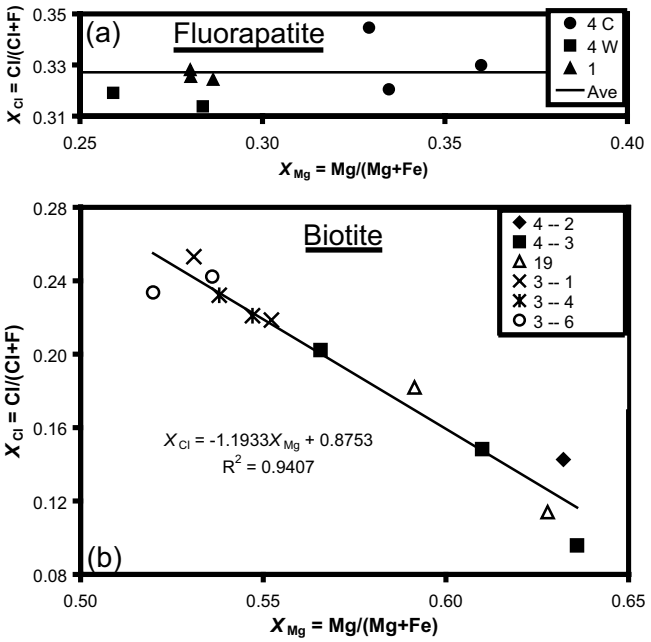

Fig. 6. Plots of Cl/(Cl+F) *vs.* Mg/(Mg+Fe) for primary fluorapatite and biotite in sample 121401E, including data from Grew *et al.* (2006). (a) Fluorapatite. Numbers in legend refer to section; C indicates spots near chopinite, W indicates spots near wagnerite. (b) Numbers in legend refer to three sections of sample 121401E (sections 4 – 2 and 4 – 3 are from the same slice as the chopinite-bearing section, but do not contain chopinite).

Table 10. Analyses of feldspars in sample 121401E.

Sect / gr	19 / 1*	19 / 1a*	10 / 2**	10 / 6
Mineral	Pl	Kfs	Pl	Kfs
No. spots	11	3	10	10
Wt%				
SiO_2	63.92	64.74	65.82	64.73
Al_2O_3	22.77	18.69	21.71	18.46
P_2O_5	0.31	0.33	0.34	0.19
Fe_2O_3	0.32	0.23	0.01	0.19
MnO	0.01	0.02	b.d.	b.d.
MgO	b.d.	0.01	b.d.	0.03
Na_2O	9.75	1.64	10.24	1.00
K_2O	0.08	14.21	0.54	14.99
CaO	3.38	0.11	1.98	b.d.
BaO	b.d.	b.d.	0.02	0.07
Sum	100.54	99.96	100.66	99.65
Formulae per 8 O				
Si	2.806	2.972	2.875	2.988
Al	1.178	1.011	1.118	1.004
P	0.012	0.013	0.013	0.008
Fe	0.010	0.008	0.000	0.007
Mn	0.000	0.001	0.000	0.000
Mg	0.000	0.000	0.000	0.002
Na	0.830	0.146	0.867	0.089
K	0.004	0.832	0.030	0.883
Ca	0.159	0.005	0.092	0.000
Ba	0.000	0.000	0.000	0.001
Sum	5.000	4.988	4.996	4.981

Notes: Sect / gr – section / grain. n.a. – not analyzed. All Fe as Fe_2O_3. Analyses done at the University of Maine. *In corona between orthopyroxene and fluorapatite (Fig. 8a). **Adjacent to K-feldspar-quartz intergrowth (Fig. 7b).

Zhang, 1995), and only one other metamorphic occurrence if "mineral A" reported from Lake Quoich, Scotland (Livingstone, 1980) is sarcopside, as suggested by its composition (Černý *et al.*, 1998). Associations of fluorapatite and sarcopside are not common, and in some cases fluorapatite is later (*e.g.* Fransolet *et al.*, 1986). The closest analogues to the Brattnevet assemblage of chopinite, wagnerite and stornesite-(Y) are assemblages of the Fe-dominant analogues, respectively, sarcopside, zwieselite, and johnsomervilleite, as well as the Mn-dominant phosphate graftonite, in granites and granitic pegmatites (*e.g.* London *et al.*, 1999; Roda *et al.*, 2004). This analogy supports the suggestion that the origin of chopinite and associated ferromagnesian phosphates is closely tied to granitic melts resulting from anatexis (Grew *et al.* 2006), a scenario we would like to further develop here based on new information obtained on the Brattnevet sample and rethinking after constructive reviews.

Table 11. Selected analyses of sapphirine, corundum, sillimanite and orthopyroxene in sample 121401E.

Sect / gr	4-2 / 1	4-2 / 3	4-2 / 3	19 / 2
Mineral	Spr	Crn*	Sil*	Opx
No. spot	10	10	10	9
wt%				
SiO_2	11.65	n.a.	36.47	48.91
P_2O_5	b.d.	n.a.	0.03	n.a.
TiO_2	0.04	0.02	0.03	0.20
Al_2O_3	61.56	98.92	61.98	5.67
V_2O_3	0.03	b.d.	0.01	n.a.
Cr_2O_3	0.02	b.d.	0.01	0.07
Fe_2O_3	3.32	1.07	1.00	n.a.
FeO	9.99	n.a.	n.a.	23.61
MnO	0.06	b.d.	0.00	0.19
MgO	13.17	b.d.	0.03	20.94
CaO	b.d.	n.a.	0.02	0.06
Na_2O	0.01	n.a.	b.d.	0.02
K_2O	b.d.	n.a.	b.d.	0.02
Sum	99.85	100.02	99.58	99.68
Formulae				
O / cations	20 / 14	3	5	6
Si	1.420	–	0.992	1.841
P	0.000	–	0.001	–
Ti	0.003	0.000	0.001	0.006
Al	8.846	1.986	1.987	0.251
V	0.003	0.000	0.000	–
Cr	0.002	0.000	0.000	0.002
Fe^{3+}	0.304	0.014	0.020	–
Fe^{2+}	1.019	–	–	0.743
Mn	0.006	0.000	0.000	0.006
Mg	2.394	0.000	0.001	1.175
Ca	0.000	–	0.000	0.002
Na	0.002	–	0.000	0.001
K	0.000	–	0.000	0.001
Sum	14.000	2.000	3.003	4.028
X_{Mg}	0.702	–	–	0.613

Notes: Sect / gr – section / grain. n.a. – not analyzed; b.d. – below detection; dash – not calculated. All Fe as FeO or Fe_2O_3, except sapphirine, for which FeO and Fe_2O_3 were calculated by stoichiometry. X_{Mg} = atomic Mg/(Mg+Fe^{2+}). *Fig. 8c,d. Analyses done at the University of Maine.

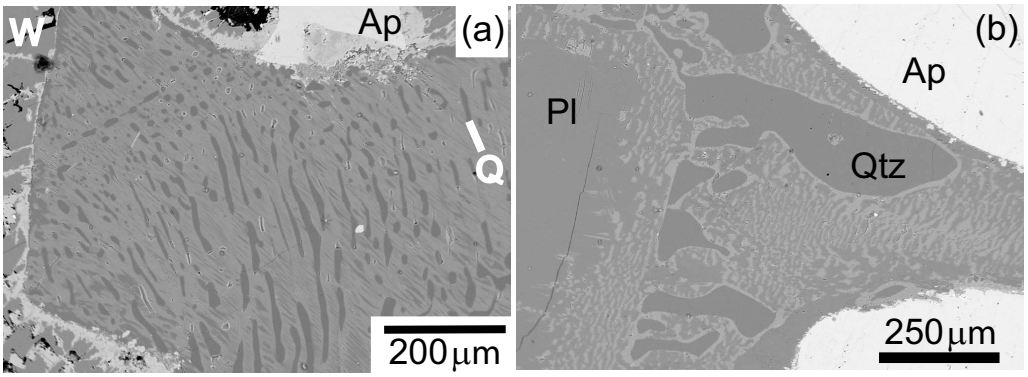

Fig. 7. Back scattered electron images of perthite-quartz intergrowths in section 121401E10. (a) K-feldspar host (light) with quartz blebs (Q, mostly vertical) and plagioclase lamellae (diagonal) surrounded by partially altered wagnerite (W). (b) Mesoperthite (light and dark) with quartz globules (Qtz) and plagioclase (Pl, Table 10). Ap – fluorapatite.

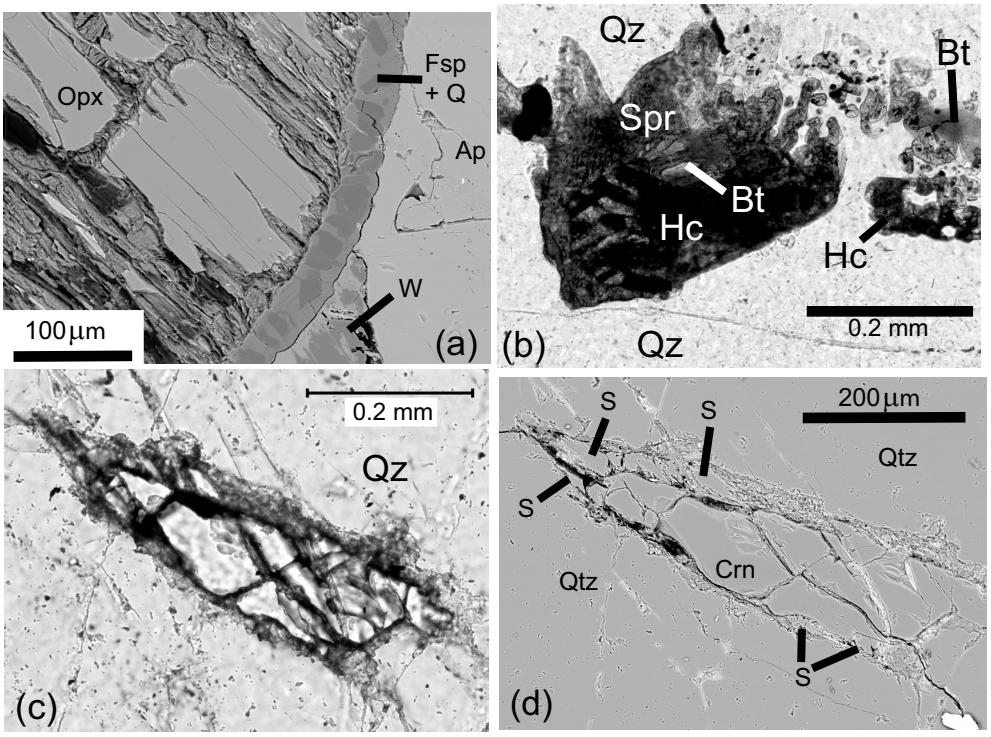

Fig. 8. (a) Back scattered electron image in section 121401E19 of orthopyroxene (Opx) partially altered to phyllosilicates, including biotite, and separated from fluorapatite (Ap) and wagnerite (W) by a corona consisting of K-feldspar (lighter), quartz and oligoclase (both darker). (b) Photomicrograph of sapphirine in direct contact with quartz in section 121401E8. Hercynite (Hc) in grain next to sapphirine is largely altered to a transparent material (diaspore?). Plane light. (c) Photomicrograph of corundum in quartz in section 121401E4 – 2 (2nd cut of slice yielding chopinite). Plane light (d) Back scattered electron image of (c) showing corundum (Crn) mantled by sillimanite (S) in quartz (Qtz). Analyses are given in Table 11. Sillimanite is partially altered to phyllosilicate, resulting in speckled material.

The scenario proposed by Grew *et al*. (2006) is based on the premise that the fluorapatite segregations and plagioclase-bearing quartz masses could be restitic bodies remaining after melt had been extracted from P-bearing biotite-plagioclase paragneiss. Additional perspective on this scenario is provided by orthopyroxene, sapphirine and corundum, all three of which were discovered in the Brattnevet specimen after the Grew *et al*. (2006) manuscript was in press. Although the first two minerals have stabilities with quartz, none has been confirmed for corundum. One possible explanation that Harlov & Milke (2002) forwarded for the juxtaposition of corundum and quartz is that the two phases formed in separate locations and were forced together by deformation; subsequent reaction between the two was sufficiently slowed by low water activities or difficulty of nucleation that only a narrow rim of sillimanite developed, armoring the corundum.

Failure to attain equilibrium could also explain the appearance of ferromagnesian phosphates in anatectic melts in which the phosphorus content was supposedly buffered by apatite. Grew *et al*. (2006) proposed that melts permeating the restitic apatite reacted with it and incorporated P. The

Table 12. Analyses of oxides in sample 121401E.

Sect / gr	19 / 1	4-2 / 2	10 / 4
Mineral	Mgt	Rt	Hc*
No. spots	10	5**	10
wt %			
TiO_2	0.09	93.49	b.d.
ZrO_2	n.a.	0.05	b.d.
SnO_2	b.d.	1.32	b.d.
Al_2O_3	0.17	0.06	57.31
V_2O_3	0.58	0.80	0.29
Cr_2O_3	0.67	b.d.	0.03
Fe_2O_3	67.79	n.a.	4.53
MgO	0.01	0.01	5.16
MnO	0.01	b.d.	0.01
FeO	31.38	1.55	32.48
NiO	n.a.	n.a.	0.14
ZnO	0.01	b.d.	0.85
Nb_2O_5	0.02	2.34	b.d.
Ta_2O_5	b.d.	0.11	b.d.
WO_3	b.d.	0.22	b.d.
Total	100.73	99.95	100.79
Formulae			
O / cations	4 / 3	2	4 / 3
Ti	0.003	0.957	0.000
Zr	–	0.000	0.000
Sn	0.000	0.007	0.000
Al	0.008	0.001	1.897
V	0.018	0.009	0.006
Cr	0.020	0.000	0.001
Fe^{3+}	1.948	–	0.096
Mg	0.000	0.000	0.216
Mn	0.000	0.000	0.000
Fe^{2+}	1.002	0.018	0.763
Ni	–	–	0.003
Zn	0.000	0.000	0.018
Nb	0.000	0.014	0.000
Ta	0.000	0.000	0.000
W	0.000	0.001	0.000
Total	3.000	1.007	3.000
X_{Mg}	0.000	–	0.221

Notes: Sect / gr – section / grain. n.a. – not analyzed; b.d. – below detection; dash – not calculated. All Fe is given either as FeO (rutile) or apportioned between FeO and Fe_2O_3 by assuming stoichiometry (Mgt, Hc). X_{Mg} = atomic Mg/(Mg+Fe^{2+}). Analyses done at the University of Maine. *Adjacent to quartz. **Except ZrO_2 (see text)

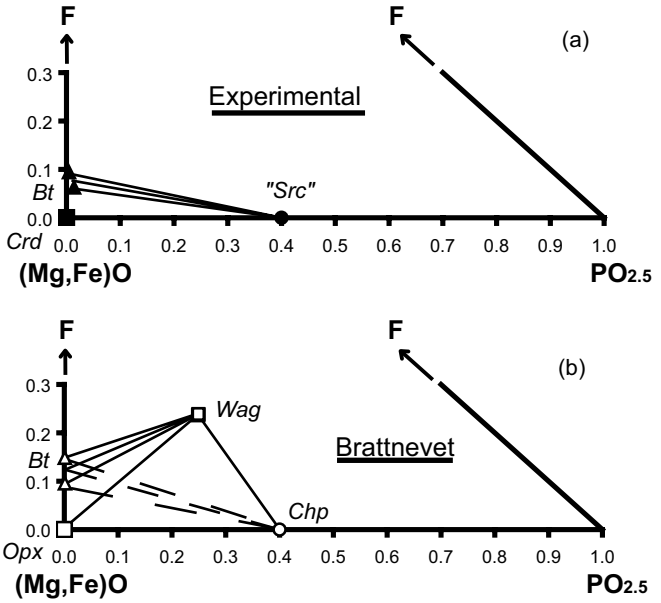

Fig. 9. Schematic relationships of phases in the (Mg,Fe)O-F-$PO_{2.5}$ system coexisting with granitic melt for (a) experiments at 2 kbar and 650–750 °C (London *et al*. 1999) and (b) Brattenevet at 6–7 kbar and 800–860 °C (Fig. 10). Silicate phase at (Mg,Fe)O corner depends on availability of SiO_2 and Al_2O_3 in the melt. The component $KAlSi_3O_8$ is presumed to be in excess, either in the melt or in K-feldspar, so that biotite compositions can be projected into this system. The maximum and minimum F contents of biotite are plotted in both diagrams.

distinctive quartz-microperthite intergrowths (Fig. 7) are inferred to be remains of this melt. Under equilibrium conditions, P and Ca content of the melt would be buffered by apatite and melt P/Ca ratio would never be great enough for ferromagnesian (or manganese) phosphates to be stabilized in addition to apatite according to the model developed by London *et al*. (1999). However, Wolf & London (1994) reported experiments in which the low diffusivity of P in granitic melts resulted in buildup of P adjacent apatite to several times the saturation, whereas Ca diffused away more quickly. These experiments suggest the possibility of high P concentrations in small melt bodies surrounded by apatite. If Ca diffused away more rapidly than P, then P/Ca ratio might have been sufficiently high for ferromagnesian phosphates to appear. Thus, the experimental results of London *et al*. (1999) on Ca-absent compositions at 650–750 °C, 2 kbar could be applied to Brattnevet [where X_F is F/(F + OH + Cl)]:

Bt (X_{Mg} = 0.47–0.68, X_F = 0.06–0.12) + Al_2SiO_5 (melt) + SiO_2 (melt) + P_2O_5 (in melt) = Kfs + cordierite (X_{Mg} = 0.72–0.82) + $(Mg,Fe)_3(PO_4)_2$ (X_{Mg} = 0.76–0.85) + H_2O (1)

The corresponding reaction for sample 121401E from Brattnevet is:

Bt (X_{Mg} = 0.52–0.67; X_F = 0.12–0.22) + P_2O_5 (in melt) = Kfs + Hc + Mgt + Ilm ± Spr ± Crn ± Opx (X_{Mg} = 0.59–0.61) + Wag (X_{Mg} = 0.92–0.93) ± Sto (X_{Mg} = 0.68–0.71) ± Chp (X_{Mg} = 0.72–0.73) + H_2O (2)

X_{Mg} of initial biotite compositions in the experiments and nature overlap, but the natural biotite is much richer in Ti (5.0–6.6 *vs.* 0.9–1.0 wt % TiO_2) and in halogens. The association of highly magnesian wagnerite with Fe-dominant oxides might balance the less magnesian synthetic cordierite + $(Mg,Fe)_3(PO_4)_2$ assemblage in terms of X_{Mg}, and Ti would account for ilmenite in the natural product assemblage. However, the natural product assemblage differs from the experimental because the most abundant phosphate is wagnerite rather than $(Mg,Fe)_3(PO_4)_2$, and cordierite is absent from the Brattnevet sample (only a trace of what could be altered cordierite was found in the Stornes specimens, Grew *et al.*, 2006).

Figure 9 compares the Brattnevet assemblage to the experimental assemblage reported by London *et al*. (1999). The appearance of wagnerite in the natural assemblage is

most likely due to greater availability of F, which is evidenced in the higher F contents in the Brattnevet biotite and is consistent with a reaction relating Chp + Bt and Wag + Opx assemblages based on simplified compositions from the Brattnevet specimen:

$$Bt + Chp + 2Qtz + 1.4F = 2Opx + 2Wag + KAlSi_3O_8 + 0.8H_2O \quad (3)$$

However, there is no evidence from fluorapatite and biotite halogen contents within the Brattnevet specimen (Fig. 6) for variation in F contents from one part of the specimen to another, and thus this reaction would not explain the appearance of chopinite in the Brattnevet specimen. Fluorapatite associated with chopinite has a higher X_{Mg} than other fluorapatite in the Brattnevet specimen (Fig. 6a), and nearby biotite is more magnesian than other biotite in the sample (*e.g.* Table 9), suggesting that increasing Mg/Fe ratio could favor Bt + Chp. However, a local increase in P could be more important than either F or Mg/Fe, *i.e.*, a shift rightward of the bulk composition in the triangles in Fig. 9. If the presence of wagnerite is due to a non-equilibrium excess of P in the anatectic melt over that resulting from fluorapatite saturation, an even greater deviation from equilibrium would be needed to attain the higher P contents necessary for chopinite formation. Stornesite-(Y) presumably also results from a localized excess of P. It is not as rare as chopinite, implying that another condition necessary for chopinite formation is localized depletion of Ca and Na.

Chopinite-farringtonite relations

Brunet & Vielzeuf (1996) and Brunet *et al.* (1998) showed that their $Mg_3(PO_4)_2$-II (chopinite) is a high-pressure polymorph of the meteoritic mineral farringtonite and predicted that Fe^{2+} would stabilize chopinite-sarcopside solid solutions to lower pressures. Calculation of isopleths (Fig. 10) requires data on Mg-Fe distribution between farringtonite and chopinite-sarcopside as well as the volume of reaction determined by Brunet & Vielzeuf (1996) and Brunet *et al.* (1998). Grew *et al.* (2006) calculated this distribution coefficient, $K_D = (Mg/Fe)_{Far}/(Mg/Fe)_{Src} = 2.30$, from the distribution coefficients between each of these two minerals and johnsomervilleite or chladniite calculated from compositions in terrestrial and meteoritic minerals (Fig. 11a). We assumed that the most magnesian compositions that McCoy *et al.* (2006) called farringtonite are indeed farringtonite. More ferroan compositions show different Fe-Mg distributions, *i.e.*, the "Mg-graftonite" of Floss (1999) behaves like sarcopside-chopinite.

The isopleth for 70% chopinite solid solution passes through the box indicating peak conditions in the Larsemann Hills, but the isopleth for 40% chopinite is 2 kbar higher than the synthesis of this composition by Charalampides *et al.* (1988) at 0.8 kbar, 500 °C (Fig. 10). This discrepancy implies the calculated K_D is too low, that is, the isopleths are too closely spaced; variation of K_D with composition could also play a role.

London *et al.* (1999) referred to their $(Mg_{0.8}Fe_{0.2})_3(PO_4)_2$ phase as "sarcopside" but cited no evidence other than composition to back this identification. Even allowing for discrepancy noted above, Fig. 10 shows that it is highly unlikely that their phase is chopinite; more likely, it is farringtonite. This identification is consistent with Mg-Fe distribution between biotite and their synthetic phosphate $(Mg,Fe)_3(PO_4)_2$: $K_D = (Mg/Fe)_P/(Mg/Fe)_{Chp} = 2.28$ (Fig. 11b), virtually identical for K_D for farringtonite-sarcopside (Fig. 11a).

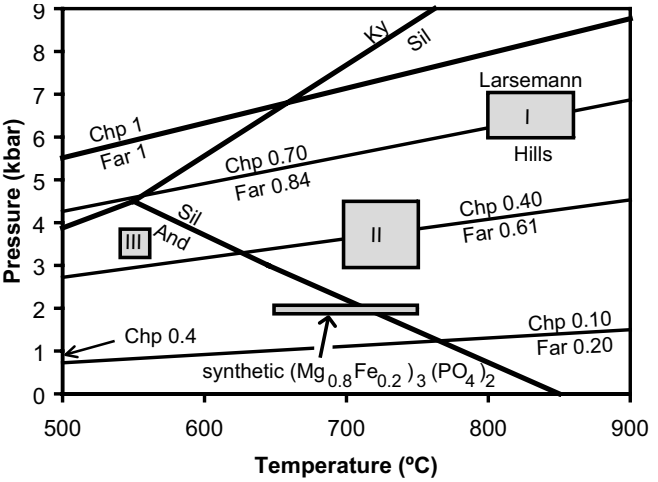

Fig. 10. Schematic pressure-temperature diagram showing isopleths calculated from the reaction and volume change in the $Mg_3(PO_4)_2$ system (Chp 1-Far 1, Brunet & Vielzeuf 1996; Brunet *et al.* 1998) for chopinite-sarcopside solid solution associated with farringtonite solid solution and assuming both solid solutions are ideal and a $K_d = (Mg/Fe)_{Far}/(Mg/Fe)_{Chp} = 2.30$ (Fig. 11a). Charalampides *et al.* (1988) synthesized sarcopside containing 40% chopinite at 0.8 kbar, 500 °C (arrow Chp 0.4). Numbered gray-filled boxes indicate peak (I) and post peak (II, III) metamorphic conditions for the Larsemann Hills based on *P-T* estimates reported for the Larsemann Hills and nearby exposures (Thost *et al.*, 1994; Fitzsimons, 1996; Carson *et al.*, 1997). Unnumbered gray-filled box indicates synthesis conditions for $(Mg_{0.8}Fe_{0.2})_3(PO_4)_2$ (average composition) by London *et al.* (1999). Al_2SiO_5 relations are from Pattison (1992). And – andalusite, Chp – chopinite, Far – farringtonite, Ky – kyanite, Sil – sillimanite.

Acknowledgments: We wish to thank the leader, Bob Jones, and other members of the 2003–2004 Australian National Antarctic Research Expedition for logistics support during the summer field season. Assisted by Michel Fialin, Christian Chopin graciously carried out analyses of his namesake, biotite, wagnerite, apatite and albite in section 121401E4 at the Centre de Microanalyse Camparis, for which we are deeply grateful. We thank Fabrice Brunet for fruitful discussions, David London for comments, and Fabrice Brunet and an anonymous referee for thoughtful reviews of the manuscript. CJC's and ESG's fieldwork in the Larsemann Hills was supported by Antarctic Science Advisory Committee Project no. 2350. ESG's and MGY's research was supported by U.S. National Science Foundation grants OPP-0228842 and MRI-0116235 to the University of Maine.

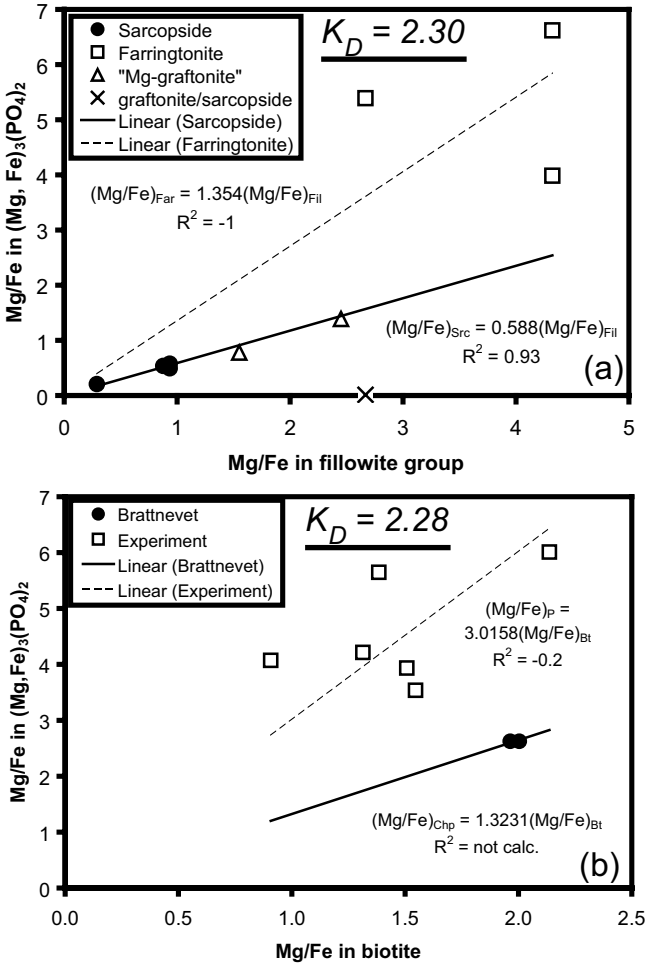

Fig. 11. Distribution of Fe and Mg between $(Mg, Fe)_3(PO_4)_2$ phases, fillowite group minerals and biotite. (a) $K_D = (Mg/Fe)_{Far} / (Mg/Fe)_{Scp}$. Sources of data: Livingstone (1980), Černý *et al.* (1998), and Corbella i Cordomí & Melgarejo i Draper (1990) for sarcopside and johnsomervilleite; Floss (1999) and McCoy *et al.* (2006) for farringtonite, "Mg-graftonite", graftonite/sarcopside and chladniite in lodranite GRA 95209. (b) $K_D = (Mg/Fe)_P / (Mg/Fe)_{Chp}$, where P is the $(Mg, Fe)_3(PO_4)_2$ phosphate reported by London *et al.* (1999) as sarcopside. Sources of data: Camparis analyses of chopinite (average from Table 6), Camparis analyses of biotite in grains 1 and 2 (Table 9), and analyses of synthetic $(Mg, Fe)_3(PO_4)_2$ and biotite from London *et al.* (1999).

References

Annersten, H. & Nord, A.G. (1980): A high pressure phase of magnesium orthophosphate. *Acta Chem. Scand.*, **A34**, 389–390.

Annersten, H., Ericsson, T., Nord, A.G. (1980): The cation ordering in iron-containing zinc and magnesium orthophosphates determined from Mössbauer spectroscopy. *J. Phys. Chem. Solids*, **41**, 1235–1240.

Armbruster, T., Bürgi, H.B., Kunz, M., Gnos, E., Brönnimann, S., Lienert, C. (1990): Variation of displacement parameters in structure refinements of low albite. *Am. Mineral.*, **75**, 135–140.

Berthet, G., Joubert, J.C., Bertaut, E.F. (1972): Vacancies ordering in new metastable orthophosphates $[Co_3\square]P_2O_8$ and $[Mg_3\square]P_2O_8$ with olivin-related structure. *Z. Kristallogr.*, **136**, 98–105.

Bild, R.W. (1974): New occurrences of phosphates in iron meteorites. *Contrib. Mineral. Petrol*, **45**, 91–98.

Brunet, F. & Vielzeuf, D. (1996): The farringtonite / $Mg_3(PO_4)_2$-II transformation: A new curve for pressure calibration in piston-cylinder apparatus. *Eur. J. Mineral.*, **8**, 349–354.

Brunet, F., Chopin, C., Seifert, F. (1998): Phase relations in the MgO–P_2O_5–H_2O system and the stability of phosphoellenbergerite: petrological implications. *Contrib. Mineral. Petrol.*, **131**, 54–70.

Buseck, P.R. & Holdsworth, E. (1977): Phosphate minerals in pallasite meteorites. *Mineral. Mag.*, **41**, 91–102.

Carson, C. J., Powell, R., Wilson, C.J.L., Dirks, P.H.G.M. (1997): Partial melting during tectonic exhumation of a granulite terrane: an example from the Larsemann Hills, East Antarctica. *J. Metamorphic Geol.*, **15**, 105–126.

Černý, P., Selway, J.P., Ercit, T.S., Breaks, F.W., Anderson, A.J., Anderson, S.D. (1998): Graftonite – beusite in granitic pegmatites of the Superior Province: A study in contrasts. *Can. Mineral.*, **36**, 367–376.

Charalampides, G., Ericsson, T., Nord, A.G., Khangi, F. (1988): Studies of hydrothermally prepared (Fe, $M)_3(PO_4)_2$-sarcopsides. *N. Jahrb. Mineral. Mh.*, 1988, 324–336.

Corbella i Cordomí, M. & Melgarejo i Draper, J.-C. (1990): Características y distribución de los fosfatos de las pegmatitas graníticas de la península del Cap de Creus (Pirineo oriental catalán). *Bol. Soc. Españ. Mineral.*, **13**, 169–182.

Fitzsimons, I.C.W. (1996): Metapelitic migmatites from Brattstrand Bluffs, East Antarctica–Metamorphism, melting and exhumation of the mid crust. *J. Petrol.*, **37**, 395–414.

Floss, C. (1999): Fe,Mg,Mn-bearing phosphates in the GRA 95209 meteorite: Occurrences and mineral chemistry. *Am. Mineral.*, **84**, 1354–1359.

Fontan, F. & Fransolet, A.-M. (1986): Les phosphates de Fe et Mn des pegmatites de Valmy, Massif des Albères (Pyrénées Orientales), France. *Bol. Soc. Españ. Mineral.*, **9**, 391–396.

Fransolet, A.-M. (1977): Intercroissances et inclusions dans les associations graftonite-sarcopside-triphylite. *Bull. Soc. Franç. Minéral. Cristallogr.*, **100**, 198–207.

Fransolet, A.-M., Keller, P., Fontan, F. (1986): The phosphate mineral associations of the Tsaobismund Pegmatite, Namibia. *Contrib. Mineral. Petrol.*, **92**, 502–717.

Fuchs, L.H., Olsen, E., Gebert, E. (1973): New X-Ray and compositional data for farringtonite, $Mg_3(PO_4)_2$. *Am. Mineral.*, **58**, 949–951.

Grew, E.S., Armbruster, T., Medenbach, O., Yates, M.G., Carson, C.J. (2006): Stornesite-(Y), $(Y, Ca)\square_2Na_6(Ca,Na)_8(Mg,Fe)_{43}(PO_4)_{36}$, the first terrestrial Mg-dominant member of the fillowite group, from granulite-facies paragneiss in the Larsemann Hills, Prydz Bay, East Antarctica. *Am. Mineral.*, **91**, 1412–1424

Grew, E.S., Armbruster, T., Medenbach, O., Yates, M.G., Carson, C.J. (2007): Tassieite, $(Na,\square)Ca_2(Mg,Fe^{2+},Fe^{3+})_2(Fe^{3+},Mg)_2(Fe^{2+},Mg)_2(PO_4)_6.2H_2O$, a new hydrothermal wicksite-group mineral in fluorapatite nodules from granulite-facies paragneiss in the Larsemann Hills, Prydz Bay, East Antarctica. *Can. Mineral.*, **45**, in press

Harlov, D.E. & Milke, R. (2002): Stability of corundum + quartz relative to kyanite and sillimanite at high temperature and pressure. *Am. Mineral.*, **87**, 424–432.

Henry, P.F., Weller, M.T., Wilson, C.C. (2003): Determination of the cation distribution in $Fe_2Ni(PO_4)_2$ using isotopic substitution and powder neutron diffraction. *J. Appl. Crystallogr.*, **36**, 1361–1367.

Hurlbut, C.S. (1965): Detailed description of sarcopside from East Alstead, New Hampshire. *Am. Mineral.*, **50**, 1698–1707.

Huvelin, P., Orliac, M., Permingeat, F. (1971): Graftonite et sarcop-

side de Sidi-bou-Othmane (Jebilet, Maroc). *Notes Serv. Géol. Maroc*, **31**, 277–284.

Larsen, E.S. & Berman, H. (1934): The microscopic determination of the nonopaque minerals. *U.S. Geol. Surv. Bull.* **848**, 266 p.

Lindberg, M.L. (1950): Arrojadite, hühnerkobelite, and graftonite. *Am. Mineral*., **35**, 59–76.

Livingstone, A. (1980): Johnsomervilleite, a new transition-metal phosphate mineral from the Loch Quoich area, Scotland. *Mineral. Mag*., **43**, 833–836.

London, D., Wolf, M.B., Morgan, G.B., VI, Garrido, M.G. (1999): Experimental silicate – phosphate equilibria in peraluminous granitic magmas, with a case study of the Alburquerque Batholith at Tres Arroyos, Badajoz, Spain. *J. Petrol*., **40**, 215–240.

Malló, A., Fontan, F., Melgarejo, J.-C., Mata, J.M. (1995): The Albera zoned pegmatite field, Eastern Pyrenees, France. *Mineral. Petrol*., **55**, 103–116.

Mandarino, J.A. (1981): The Gladstone – Dale relationship: Part IV. The compatibility concept and its application. *Can. Mineral*., **19**, 441–450.

McCoy, T.J., Carson, W.D., Nittler, L.R. Stroud, R.M. Bogard, D.D., Garrison, D.H. (2006): Graves Nunataks 95209: A snapshot of metal segregation and core formation. *Geochim. Cosmochim. Acta*, **70**, 516–531.

Medenbach, O. (1985): A new microrefractometer spindle-stage and its application. *Fortschr. Mineral*. **63**, 111–133.

Merlet, C. (1994): An accurate computer correction program for quantitative electron-probe microanalysis. *Mikrochimica Acta*, **114**, 363–376.

Moore, P.B. (1972): Sarcopside: its atomic arrangement. *Am. Mineral*., **57**, 24–35.

Nord, A.G. (1984): Crystallographic studies of olivine-related sarcopside-type solid solutions. *Z. Kristallogr.*, **166**, 159–176.

Nord, A.G., & Kierkegaard, P. (1968): The crystal structure of $Mg_3(PO_4)_2$. *Acta Chem. Scand.*, **22**,1466–1474.

Olsen, E.J., Kracher, A., Davis, A.M., Steele, I. M., Hutcheon, I.D., Bunch, T.E. (1999): The phosphates of IIIAB iron meteorites. *Meteoritics & Planetary Science*, **34**, 285–300.

Palache, C., Berman, H., Frondel, C. (1951): The System of Mineralogy of James Dwight Dana and Edward Salisbury Dana, Yale University. 7th ed, v. II. Halides, Nitrates, Borates, Carbonates, Sulfates, Phosphates, Arsenates, Tungstates, Molybdates, etc. Wiley, New York, 1124 p.

Pattison, D.R.M. (1992): Stability of andalusite and sillimanite and the Al_2SiO_5 triple point: Constraints from the Ballachulish aureole, Scotland. *J. Geol.*, **100**, 423–446.

Povondra, P., Pivec, E., Čech, F., Lang, M., Novák, F., Prachař, I., Ulrych, J. (1987): Přibyslavice peraluminous granite. *Acta Univ. Carol., Geol.*, **3**, 183–283.

Roda, E., Pesquera, A., Fontan, F., Keller, P. (2004): Phosphate mineral associations in the Cañada pegmatite (Salamanca, Spain): Paragenetic relationships, chemical compositions, and implications for pegmatite evolution. *Am. Mineral.*, **89**, 110–125.

Sheldrick, G.M. (1997) SHELXS97 and SHELXL97. University of Göttingen, Germany..

Smeds, S.-A., Uher, P., Černý, P., Wise, M.A., Gustafsson, L., Penner, P. (1998): Graftonite – beusite in Sweden: Primary phases, products of exsolution, and distribution in zoned populations of granitic pegmatites. *Can. Mineral*., **36**, 377–394.

Stalder, M. & Rozendaal, A. (2002): Graftonite in phosphatic iron formations associated with the mid-Proterozoic Gamsberg Zn-Pb deposit, Namaqua Province, South Africa. *Mineral. Mag*., **66**, 915–927.

Thost, D. E., Hensen, B. J., Motoyoshi, Y. (1994): The geology of a rapidly uplifted medium and low pressure granulite facies terrane of Pan-African age: the Bolingen Islands, Prydz Bay, Eastern Antarctica. *Petrology*, **2**, 293–316.

Warner, J.K., Cheetham, A.K., Nord, A.G., von Dreele, R.B., Yethiraj, M. (1992): Magnetic structure of iron (II) phosphate, sarcopside, $Fe_3(PO_4)_2$. *J. Materials Chem.*, **2** (2), 191–196.

Watson, E.B., Wark, D.A., Thomas, J.B. (2006): Crystallization thermometers for zircon and rutile. *Contrib. Mineral. Petrol*., **151**, 413–433.

Wolf, M.B. & London, D. (1994): Apatite dissolution into peraluminous haplogranitic melts: An experimental study of solubilities and mechanisms. *Geochim. Cosmochim. Acta*, **58**, 4175–4145.

Yvon, K., Jeitschko, W., Parthe, E. (1977): LAZY PULVERIX, a computer-program, for calculating X-ray and neutron-diffraction powder patterns. *J. Appl. Crystallogr.*, **10**, 73–74.

Zack, T., Moraes, R., Kronz, A. (2004): Temperature dependence of Zr in rutile: empirical calibration of a rutile thermometer. *Contrib. Mineral. Petrol*., **148**, 471–488.

Zhang, R. (1995): Mg-sarcopside, a new variety of sarcopside group. *Kuangwu Yanshi = J. Mineral. Petrol.*, **15**, 6–10 (in Chinese with English abstract).

Zhu, C. & Sverjensky, D.A. (1992): F-Cl-OH partitioning between biotite and apatite. *Geochim. Cosmochim. Acta*, **56**, 3435–3467.

Received 22 July 2006
Modified version received 21 November 2006
Accepted 18 December 2006